We are IntechOpen, the world's leading publisher of Open Access books Built by scientists, for scientists

4,800
Open access books available

122,000
International authors and editors

135M
Downloads

Our authors are among the

154
Countries delivered to

TOP 1%
most cited scientists

12.2%
Contributors from top 500 universities

CLARIVATE ANALYTICS BOOK CITATION INDEX INDEXED

WEB OF SCIENCE™

Selection of our books indexed in the Book Citation Index in Web of Science™ Core Collection (BKCI)

Interested in publishing with us?
Contact book.department@intechopen.com

Numbers displayed above are based on latest data collected.
For more information visit www.intechopen.com

Chapter 23

Microclimate and Indoor Air Quality in an Operating Theatre under real use Conditions — An Experimental and Numerical Investigation

Carla Balocco and Giuseppe Petrone

Additional information is available at the end of the chapter

http://dx.doi.org/10.5772/59671

1. Introduction

The study of OT ventilating and IAQ conditions is particularly important. Campaigns of experimental measurements in OTs are usually expensive, invasive and, in many countries, require complex procedures for legal authorization. CFD simulation has opened up low cost methods to provide useful indications on proper indoor microclimate conditions and IAQ. [1, 2,3]. There is a great dealing the literature on airflow patterns, air velocity and temperature distribution in unidirectional (vertical downward) airflows, as well as other applied ventilating layouts, such as air curtains use to achieve a chosen air quality level inside OTs using CFD transient simulations [4,5,6,7,8]. Other authors have studied the airflow and temperature distribution modifications due to different surgical lamp shapes and locations [9]. In particular [10], the effectiveness of the ventilation system and airborne bacteria removal due to the HVAC plant have been analysed by means of CFD simulation supported by experimental data obtained in a test room. A comprehensive experimental and numerical analysis has been proposed by Kameel and Khalil [11] concerning both the airflow regimes and heat transfer inside an OT considering the correct operational use conditions. Few analyses have been made concerning the effect of moving objects on OT airflow: the "computationally expensive" moving mesh approach has been applied in order to manage the fluid-solid interface during transient simulations [12,13], but similar investigations were proposed for a hospital isolation room [14,15] and an industrial cleanroom [16]. An impressive study concerning the influence of movements on contaminant transport has been proposed by Brohus et al. [17] using the indirect approach, based on distributed momentum and turbulent kinetic energy sources. Recently, the present authors proposed an alternative indirect numerical approach in order to simulate solid objects moving on a fixed mesh in forced [18] and natural convection flows [19].

Definition and quantification of the contaminant sources under OT effective use conditions is a complex task. Existing databases refer to constant particle mass emission of a person as a function of his/her activity. Several studies analyze different sources and human activities causing high levels of indoor particle concentration, diffusion and re-suspension processes. Some authors [20] present studies on the influence of periodic bending movement of the surgeon on the air flow field and bacteria carrying particle distribution using a combined approach based on an Eulerian RANS model, modified drift-flux and moving mesh. In the study by Brohus et al. [17], bacteria attributed to the skin flake emission of staff and patient are simulated as a gaseous contaminant. The most widely used experimental methods allow particle size calculation for discrete intervals, so as to check whether microclimatic and IAQ conditions are in compliance with standards and specific rules. Some authors have developed a useful method for determining individual emission rates from ambient air contaminant concentrations caused by multiple indoor sources [21]. Other studies provide a sampling method integrated with statistical analysis. [22]. In a recent paper bacteria sources are investigated [23] in a university classroom both occupied and vacant as concentration differences due to the two conditions. Besides the influence of the airflow pattern, it has been demonstrated that particle dynamic behaviour is strongly dependent on particle size and size-related forces [24]. Chih-Shan Li et al. [25] carried out a series of field tests by active and passive sampling of air and surface measuring bacterial and fungal concentrations without referring to particle size and diameter. Another paper [26] based on particle counting combined with statistical analysis, evaluates aerobic bacterial sedimentation and connected index of microbial air contamination. There, results refer to different particle diameters but not emission sources. Some authors [1] have carried out transient simulations using the Renormalization Group (RNG) k-ε turbulence model, assuming a released rate of bacteria-carrying airborne particulates from surgical staff of 100 BCP/min per person and for patients of 400 BCP/min per wound. In general, CFD simulation concerning aerosol particle transport and diffusion processes can be solved by three main different numerical approaches: the first method consists in solving the particle concentration field by using diffusion-transport equations based on "passive scalar transport" in which the vector of particle transport is the motion field of the fluid but gravitational effects and frictional forces on particle motion are disregarded; the second is the Eulerian-Eulerian method and the third is the Eulerian-Lagrangian one. These last two methods solve the airflow field based on the Eulerian approach, but the particle phases are treated differently: in the first, particle concentration is directly solved using gravitational effect in the transport term, in the second one an ordinary differential equation is solved for any particle path. A modified drift-flux model based on the second approach has been applied to modelling particle transport [27,28,20]. At present, there are not many studies in the literature concerning numerical modelling in which the contaminant concentration for the IAQ analysis has been performed starting from sources of particle emission with a distribution dependent on particle diameter [29,30]. However, Italian and international standards require, for environment classification, a particle count for diameter dimension. Actually, there is a lack of data concerning specific emission sources in terms of particles issued in time unit by people. A recent study provides the quantification of size-resolved particle concentrations in indoor air of a classroom under occupied and vacant conditions [29]. Another important

http://dx.doi.org/10.5772/59671

numerical study provides information on airflow, particle deposition and movement in two different spaces equipped with displacement and mixing ventilation modes [30]. In our present research airflow and climate in an existing orthopaedics OT under both the "at rest" and real use conditions were investigated by experimental measurements and numerical simulations. The "operational" conditions should be understood with faked surgery, split into two conditions respectively "correct operational use" and "incorrect operational use". Two main purposes were pursued in our investigation: the first one consists in exploiting the experimental acquisitions in order to check whether the environmental parameters respect standard requirements. Numerical results are then correlated with the microclimatic parameters suggested by the standards to verify the model suitability for assessing the OT indoor climate according to suggested standard limits, starting from the design variables of the room and HVAC system. The second purpose focuses on the airflow and microclimatic parameter variations induced by the operative use conditions. Our study develops an investigation and applied research to obtain a distribution of emitted particles as a function of their diameter, assuming that the amount of particle mass emitted by a person in a time unit does not change with their size. Starting from this assumption, the distribution of emitted particles will consist of a larger number of a smaller size, and vice versa. Our study investigates the thermo-fluid dynamics combined with the analysis of the concentration of diluted gas phase and particle aerosol dispersion in the air. Some IAQ indexes, widely used in the literature, were calculated as global and local values referring to the total volume of the room but also to the critical zones defined by ANSI/ASHRAE [31]. The present investigation is organized, referring to air flow and climate, ventilation efficiency and IAQ in the investigated real OT, as follows: the second section presents the experimental measures; the third one concerns the numerical tools and model validation; results are reported in the fourth section; then, conclusions, basic findings and possible developments due to the application of our proposed approach to similar cases, follow.

2. Materials and methods

2.1. Experimental measurements and data analysis

Experimental measurements were conducted in a real orthopaedic OT of the University Hospital of Parma (Italy) referring to [32,33] and during the different conditions as given: **at rest**, i.e. room with all services functioning and equipment installed and operable/operating, but without surgical/healthcare staff and the patient; **operational "correct use condition"** reproducing the effective use conditions of the OT, with all services and equipment functioning, surgical and healthcare presence. Experimental data were collected after installation of all acquisition equipment in the room and during simulated hip surgery lasting 20-25 minutes and involving some PhD students. The surgical staff and healthcare assistants were in upright stationary positions and surrounding the patient lying on the operating table. The sliding door was closed; **operational "incorrect use condition"**, i.e. the same conditions described for operational "correct use", but considering the sliding door opening and closing and one healthcare assistant walking from outside through the door and up to the patient's head on

the operating table, and then turning round and moving back to the corridor. The HVAC system was working during all tests, supplying a constant incoming airflow rate at controlled temperature. The measurements campaign was carried out over a two day period, from 8 a.m. to 2 p.m. Microclimate parameters were measured over time at discrete points PT01, PT02, PT03 that are shown in Figure 1. In particular: 1 hot wire anemometer, 1 air-temperature and humidity sensor and 1 globe thermometer were set below the central air inlet diffuser on the plane of the surgical table (PT01); 1 air temperature and humidity sensor and 1 differential pressure sensor near the sliding door on a tripod (PT02); 1 differential pressure sensor and 1 air temperature and humidity sensor were set near the air outlet diffuser on a utility pole (PT03). Differential air pressure, between monitored room and the adjoining ones, was evaluated in proximity to the sliding door, at 1 m with respect to the floor. Some telescopic tripod poles were used for instrument arrangement during tests. Instruments were connected to a radio master R-Log data logger system. Measurements were made every two seconds. In Table 1 the average values of experimental measures upon N samples ($EXP_{AV} = 1/N \sum_{i=1}^{N} EXP_i$) are shown for the different room conditions. Data dispersion with respect to the average values was quantified by means of the sample standard deviation $\sigma_{(N-1)}$, computed using Bessel's correction and the percentage deviation with respect to the average value is also shown in Table 1. For air active sampling, a particle counter (Climet CL 754) was used. The equipment can sample a volume of 75 l/min of air and gives the number of suspended particles, divided according to the diameter (≥0.3; ≥0.5, ≥1.0; ≥5.0 μm), allowing one to deduce particle concentration in the diameter ranges (0.3-0.5 μm); (0.5-1 μm); (1-5 μm). Experimental data of air temperature and relative humidity (RH) are globally consistent: standard deviations are narrow, much more for temperature (less than 1 °C) than for RH (less than 3 percentage points); normalized deviation does not exceed a 6% threshold in any cases. At point PT01 a detected dispersion of experimental data appears, that becomes very significant for air velocity measurements. The higher variation of the measured velocity in PT01 during operational conditions, due to medical staff movement, produces an increase in RH levels in the central zone (PT01). Temperature values, recorded during operational conditions, are slightly lower than values in at rest conditions, because the local ventilation system operates in the full working phase. Analysing particle concentration measurements, excluding PT1 at operational conditions for particles of 0.3 μm diameter and PT05 at rest conditions for particles of 5 μm diameter, particle distribution for each diameter is similar for the two OT use conditions at the different measurement points.

As expected, the highest particle concentration values are during operational conditions. Referring to the absolute value, the higher differences between the two OT use conditions were checked at PT05 for each particle diameter, while the lower differences were checked at PT01. Particle concentration measured at PT01 for the two use conditions of OT and for each diameter, respects the standard limit imposed by the ISO5 at rest classification [34,35] and Grade B EU-GMP clean-room classification (Annex1), in accordance with EN ISO 14644, for both at rest and operational conditions. Referring to the GMP at operational conditions, at PT01 the conditions imposed by Grade B are respected by all the various particles (for all different

http://dx.doi.org/10.5772/59671

	T [°C]			T_{mr} [°C]	U [m/s]	ϕ [%]			
	PT01	PT02	PT03	PT01	PT01	PT01	PT02	PT03	
EXP_{AV}	**21.2**	**21.4**	**21.3**	**21.6**	**0.29**	**63.2**	**61.5**	**61.9**	**At rest**
$\sigma_{(N-1)}$	0.76	0.33	0.42	0.43	0.03	2.70	1.08	1.45	
$\iota = \sigma_{(N-1)}/EXP_{av}$	*3.6%*	*1.5%*	*2.0%*	*2.0%*	*10.9%*	*4.3%*	*1.8%*	*2.3%*	
EXP_{AV}	**20.1**	**21.1**	**21.1**	**20.9**	**0.23**	**65.6**	**61.8**	**62.1**	**Operational "correct use"**
$\sigma_{(N-1)}$	1.03	0.41	0.44	0.59	0.07	2.91	1.32	1.10	
$\iota = \sigma_{(N-1)}/EXP_{av}$	*5.1%*	*1.9%*	*2.1%*	*2.8%*	*29.3%*	*4.4%*	*2.1%*	*1.8%*	
EXP_{AV}	**20.1**	**21.3**	**21.2**	**20.9**	**0.28**	**67.1**	**61.8**	**62.1**	**Operational "incorrect use"**
$\sigma_{(N-1)}$	0.71	0.30	0.35	0.74	0.08	2.71	0.97	1.45	
$\iota = \sigma_{(N-1)}/EXP_{av}$	*3.6%*	*1.4%*	*1.6%*	*3.6%*	*30.0%*	*4.0%*	*1.6%*	*2.3%*	

Table 1. Microclimatic parameters measured at the discrete points for different conditions: average values (EXP_{av}), sample standard deviation ($\sigma_{(N-1)}$) and percentage error (ι).

diameters) at operational conditions, and the concentration of 0.5 μm diameter particles is within the standard limits for operational conditions, but in particular at PT01, PT03, PT04 and PT05, it is higher.

2.2. Numerical modelling

A solid model of the OT was made: the OT geometry is outlined by a rectangular-shaped room with smoothed corners, a 43 m^2 base area and 120 m^3 volume (Figure 1).

A sliding door 1.4 m wide and 2.2 m high connects the room to an entry corridor. The locations of the staff members, surgical lamps and equipment for the operating table, defined in the model are shown in the same Figure 1. The surgical staff and patient bodies are outlined as rectangular solid boxes. The room is equipped with an operating bed and lighting system made up of three joined arms, each one holding three lamps. Two further solid boxes represent an operating trolley and an electro-medical device. One of the walls of the room has a window, facing an internal space. There are two rectangular supply ceiling diffusers each of 0.56 m^2 surface, located in the central zone of the ceiling, that strengthen the unidirectional flow. Each diffuser provides a constant flow rate of 3969 m^3h^{-1} of fresh air, so that there are 66 total air changes per hour in the room. Although the real HVAC system is temperature-controlled by a remote ambient thermostat located inside the room, in the numerical models a constant inlet temperature value is set for the incoming fresh air. Two groups of 14 conical outgoing grilles (cross-section of 0.0128 m^2) are arranged over two of the opposite four walls corresponding to the OT smoothed corners. Following the indications given in the standards [36,37], the global OT air-volume (TV) is divided into 3 zones, labelled from now on as Breathing Zone (BZ, pink

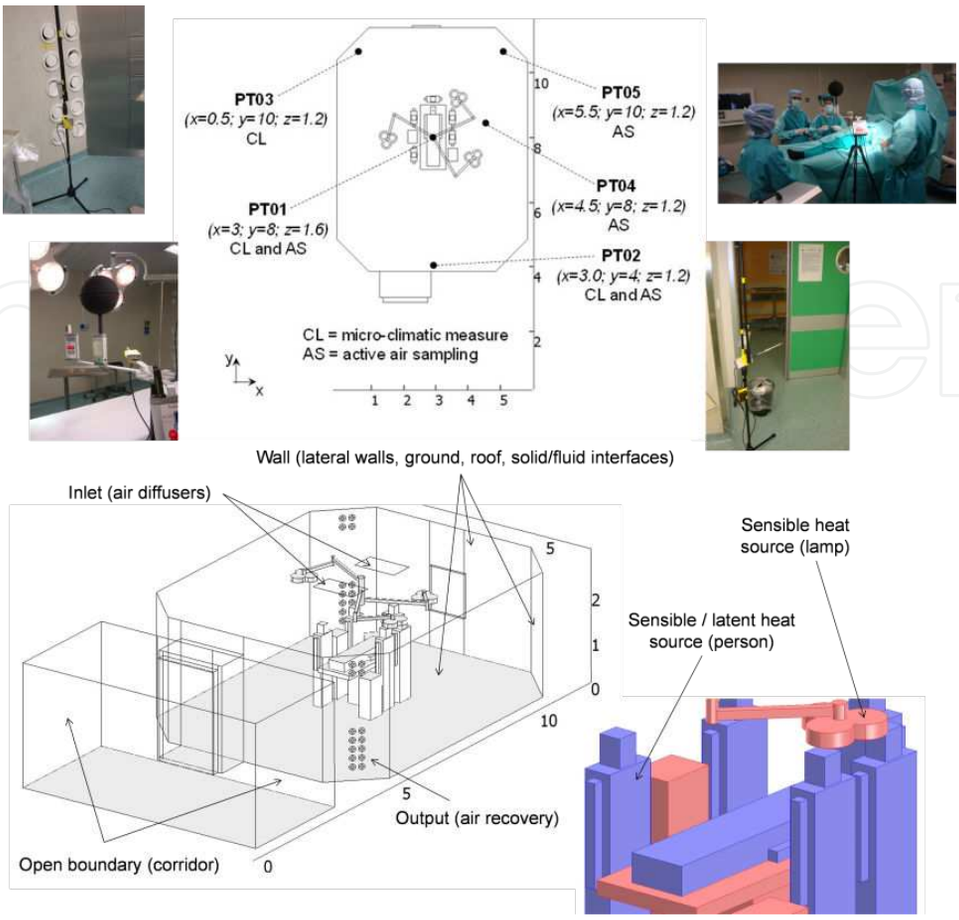

Figure 1. System description: in the map (upper portion of the figure) positions (labelled as PT01, PT02, PT03, PT04 and PT05) where instruments were located are shown; some photos taken during the experimental campaign are provided. In the bottom portion, the geometry of the numerical model: solid elements used for simulating people, room furnishing (operating table, trolleys) and equipment (ceiling diffusers, lighting system) are shown as well as some indications about physical constraints for the system.

in Figure 2), Occupied Zone (OZ, blue in Figure 2) and Peripheral Zone (PZ, corresponding to TV-OZ). This allowed the computation of air quality indexes for each zone. Numerical models were built-up to simulate airflows, climate and air quality conditions in the real orthopaedic OT used for experimental measurements.

Commercial software, that allows multi-physical analyses through solution of the related governing equations by a Finite Element approach [38], was used. Fluid-dynamics and thermal analysis were firstly solved under the assumption of Newtonian fluid and incompressible flow. A standard k-ε closure scheme [39] was used for solving velocity and pressure field by an eddy viscosity approach. Then, further transport-diffusion equations were considered for solving RH, CO_2 concentration, mean age of air and particulate concentration for diameters 0.4, 0.75, 3 μm. These dimensions represent the average particle diameter referring to the particle diameter range that were experimentally measured ((0.3-0.5 μm); (0.5-1 μm); (1-5 μm)). The basic formulation of the PDE used for computations is:

http://dx.doi.org/10.5772/59671

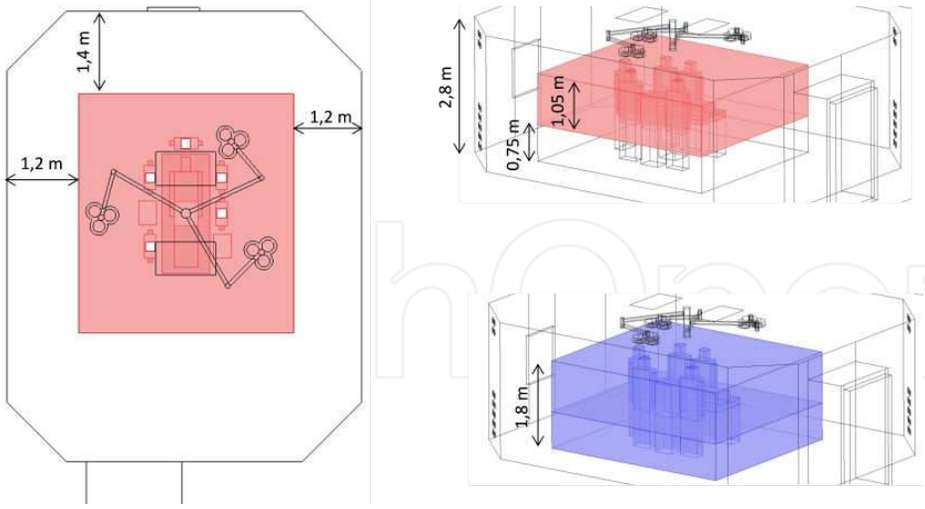

Figure 2. OT zones description: BZ (pink) and OZ (blue).

$$\frac{\partial(\rho\phi)}{\partial t} + \nabla\cdot(\rho\phi\mathbf{U}) = \nabla\cdot(\Gamma\nabla\phi) + \Lambda \tag{1}$$

where ρ is the fluid density and **U**(u, v, w) is the air velocity vector. Table 2 shows the analytical formulation of different terms in eq. (1), depending on the specific physics referred to. From a physical point of view, source term F corresponds to the buoyancy force, Q_S is the metabolic sensible heat and Q_L the latent one. For comparing room ventilation performance in different conditions, the mean age of air (τ) was computed: it quantifies the average lifetime of air at a particular location of the room [41,42,43] once a steady state is achieved in terms of airflow patterns. In solving the particulate concentration, because we considered diameters higher than 0.01 μm, the Brownian diffusivity was disregarded with respect to turbulent diffusivity, that was assumed to be equal to the air kinematic turbulent viscosity [44]. Adopting an Euler approach, the following settling velocity was added to the transport vector vertical component:

$$\mathbf{w}_S = \frac{C_c\rho_p d_p^2}{18\mu}\cdot\mathbf{g} \tag{2}$$

with C_c the Cunningham coefficient, ϱ_p and d_p particulate density and diameter, respectively. Source terms and physical properties values used in governing equations are listed in Table 3.

Equation	ϕ	Γ	Λ
Continuity	1	0	0
Momentum	$\mathbf{U}$	$\mu + \mu_T$	$-\nabla p + \mathbf{F}$
Turbulent kinetic energy	k	$\mu + \frac{\mu_T}{\sigma_k}$	$\frac{1}{2}\mu_T\left[\nabla\mathbf{U} + (\nabla\mathbf{U})^{\mathrm{T}}\right]^2 - \rho\varepsilon$
Dissipation rate of kinetic energy	ε	$\mu + \frac{\mu_T}{\sigma_\varepsilon}$	$\frac{1}{2}C_{\varepsilon 1}\frac{\varepsilon}{k}\mu_T\left[\nabla\mathbf{U} + (\nabla\mathbf{U})^{\mathrm{T}}\right]^2 - \rho C_{\varepsilon 2}\frac{\varepsilon^2}{k}$
Energy	T	$\frac{\lambda}{C_p}$	$\frac{Q_S}{C_p}$
Relative humidity	RH	$\frac{\delta_p p_{sat}}{\xi} + D_w$	$\frac{Q_L}{\xi}$
Mean age of air	τ	Υ	ρ
CO_2 concentration	CO_2	$\frac{D_{CO_2}}{\rho}$	0
Particulate concentration	C_{d_i}	$\frac{D + \varepsilon_p}{\rho}$	0

Table 2. Analytical formulation of terms in eq. (1), depending on the specific physics referred to.

	ρ	η	λ	C_p	F	Q_S	Q_L
Material	[kg/m^3]	[Pa s]	[W/(m K)]	[J/(kg K)]	[N/m^3]	[W]	[W]
Glass (window, lamp)	2500	-	1.00	800	-	4025 (lamps)	-
Wood (door)	500	-	0.50	1000	-	-	-
Aluminium (operating table, electro-medical case, lamp arms)	2700	-	160	900	-	-	-
Medical staff	950	-	0.62	4180	-	73.3	58.6
Patient	950	-	0.62	4180	-	65.9	30.7
Air	$p/(RT)$	2E-5	0.04	1004	$\rho g \beta \Delta T$	-	-

Table 3. Physical properties of materials and source term values.

Movements of the sliding door and of one healthcare assistant were numerically simulated to study the incorrect operational use conditions. In transient analyses, once the sliding door is open, one assistant is expected to walk from the corridor space inside the room, moving along the surgical table up to the patient's head, then turning around and leaving the room. The mean velocity values applied for a person walking and door opening/closing are respectively 0.7 m s^{-1} s and 0.28 m s^{-1}. The procedure adopted for simulating the "moving objects" inside the room was presented in detail in recent studies by the authors [18,19]. It is mainly based on the definition of specific source terms in the governing equations, assuming assigned values in the portions of the computational domains where the solid objects are located at a chosen time. Solid objects were not explicitly designed in the geometrical model because their movement is driven by assumed values 0 or 1 in specific logical functions during time. Solid

http://dx.doi.org/10.5772/59671

object time-displacements and paths considered during transient analyses are shown in Figure 3. The black line represents displacement of the "moving object" sliding door (x direction into the model reference system), while the red line indicates movement belonging to the "moving object" healthcare assistant (y direction). The grey dashed lines schematically separate the different steps characterizing the simulated dynamics, that are highlighted by progressive numbers from 1 to 7, as shown in the grey horizontal bars in the upper part of Figure 3. Assuming the initial instant with the door closed and medical assistant standing still in front of it, in the corridor, 7 consecutive steps were simulated: step1 (0-5 seconds): sliding door opens, and medical assistant is standing still, waiting for the door to open; step 2 (5-11 seconds): the door is completely open and medical assistant is walking through it. After 1 second, the door starts to close, while the person is walking in the room; step 3 (11-15 seconds): the door is closed and medical assistant walks through the room until he reaches the operating table top; step 4 (15-27 seconds): medical assistant stops for 3 seconds, then moves in the opposite direction towards the sliding door and finally stops inside the room in front of the door waiting for it to open; step 5 (27-32 seconds): medical assistant is standing still until the door is completely open; step 6 (32-33 seconds): the door is completely open and the person is walking through it and then stopping in the corridor; step 7 (33-38 seconds): sliding door closes.

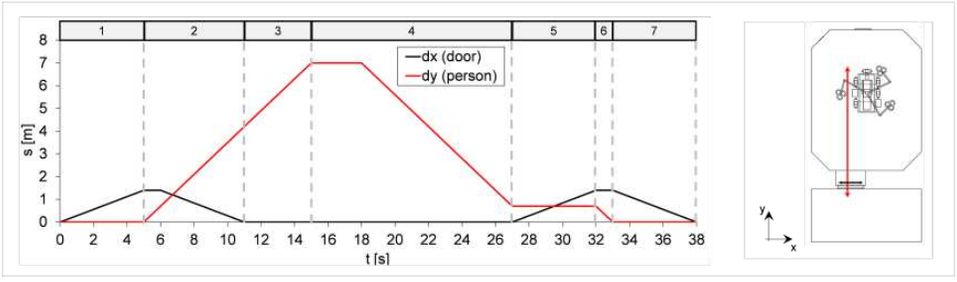

Figure 3. Path on the room map (right side) and time-displacement (left side) of the "moving objects": the black line identifies the transient position of the sliding door (moving along the x-axis in the chosen system of coordinates), the red one refers to the healthcare assistant (moving along the y-direction). The grey dashed lines separate the different steps characterizing the simulated dynamics (numbers in the grey horizontal bars).

The computational domain, representing the corridor, was considered only for simulations involving the sliding door opening/closing (incorrect use conditions). In this case, open boundary conditions were considered at the corridor transversal section. The following first-type boundary conditions for supplied air at the ceiling diffusers were assumed: velocity magnitude (1.97 m/s), turbulence intensity (5%), air temperature (18 °C), RH (60%), CO_2 concentration (350 ppm) and mean age of air (0 s). For modelling persons breathing, a RMS value, corresponding to the sinusoidal trend for inhaled/expired air, and for CO_2 emission rate into the room were assumed. Adopted values in simulations were 2.0 m^3/h (medical staff) and 0.3 m^3/h (patient) for breathed airflow and 0.080 m^3/h (medical staff) and 0.012 m^3/h (patient) for CO_2 emission rate. Outflow conditions were considered for all dependent variables at the recovery grids. At each solid/fluid interface, logarithmic wall functions were applied in the near wall airflow, that was considered parallel to the wall and being in a wall offset equals one hundred viscous units. Turbulent production was established equal to dissipation at walls.

For the remaining dependent variables impermeable/insulation conditions at walls were imposed. The occupants contribution for particle emission rate was applied as a boundary flux [particle/(m^2 s)] at the occupants/surrounding air interfaces. The procedure adopted to assess the particulate flux depending on particle dimension is explained in the next section of the present chapter. In thermal analysis, a convective thermal flux was applied to the walls, considering a heat exchange coefficient of 7.7 (W/(m^2 K)) and a constant temperature of 20 °C in the adjacent rooms. Insulation conditions were applied to the solid/fluid interfaces for all other dependent variables that were solved. For the "at rest" conditions, the lamps were considered the only internal sources of sensible heat. Otherwise, in operational "correct use" conditions, internal heat sources were related to medical staff and patient presence, as sensible and latent heat loads. Other boundary conditions were not considered to change from "correct use" to "incorrect use" operational conditions: heat and vapour source values were unchanged, except for the additional load due to the walking healthcare assistant, whose location was variable in accordance with the moving object position during time. The governing equations together with their boundary conditions were spatially discretized on non-structured grids, made of second order tetrahedral elements. Steady state solutions of discrete equations were carried-out by applying an iterative dumped Newton-Raphson scheme [45] based on the discretized PDE linearization by a first-order Taylor expansion. Algebraic systems of equations coming from differential operator discretization were solved by a PARDISO package, a direct solver particularly efficient to solve unsymmetrical sparse matrixes by a LU decomposition method. The convergence criterion was set to 1E-5. Time integration of governing equations for transient simulations was performed applying an Implicit Differential-Algebraic (IDA) solver [46], which uses variable-order and variable-step-size Backward Differentiation Formulas (BDF). Because the time-matching scheme is implicit, a nonlinear system of equations was solved at each time step. All computations were carried out on a workstation with two 64-bit 6-core/12-thread processors speeding up to 2.3 GHz of frequency and handling 128 GB of RAM.

3. Use of microclimatic measurements for numerical model validation

The influence of mesh refinement on results deviation was investigated to assure mesh independent results and assess the model reliability. Simulations were carried out in conditions labelled as "at rest". The accuracy and independence of results from mesh refinement were estimated by evaluating result variation (magnitude of air velocity and temperature) at point PT01 (see Figure 1), by increasing the number of elements of the computational grid. Table 4 provides the absolute deviation and normalized variance of the values compared to those obtained using the finest mesh (M4). It can be gathered that over a certain value of mesh refinement, the relative variance is lower than 2.5% for the velocity magnitude, i.e. the most sensitive variable with respect to mesh size. Numerical results were also compared with experimental data to check and validate the numerical model. Comparisons were made in points where probes were located (PT01, PT02, PT03). An extract of comparison is given in Figure 4a-c, where experimental and numerical results obtained for operational "correct use conditions" are compared with each other. In this figure the average value of the acquired data

http://dx.doi.org/10.5772/59671

(EXP_{AV}) and the numerical result obtained in steady state conditions (NUM), were plotted together. The experimentally detected absolute deviation above ($EXP_{MAX} - EXP_{AV}$) and below ($EXP_{AV} - EXP_{MIN}$) the average value is presented by means of error bars. In the same diagrams, circled symbols to indicate the maximum difference between acquired data and simulations ($\max_i\{|EXP_i - NUM|\}$), and squared symbols to present the difference between experimental average data and numerical results ($|EXP_{AV} - NUM|$) were used. Deviations were normalized using experimental average values as reference for temperature and velocity (Figure 4a and 4c), while the absolute values of deviation for RH (Figure 4b) was retained.

Mesh #		**M1**	**M2**	**M3**	**M4**
Number of elements		517633	774 220	1092784	1714306
Mesh refinement		-	33%	29%	36%
Velocity magnitude in (3; 8; 1.4)	[m/s]	0.303	0.305	0.309	0.316
Absolute gap	[m/s]	0.013	0.012	0.007	0.000
Relative gap	[-]	4.2%	3.74%	2.20%	0.00%
Temperature in (3; 8; 1.4)	[°C]	20.145	20.154	20.156	20.156
Absolute gap	[°C]	0.011	0.002	0.000	0.000
Relative gap	[-]	0.05%	0.01%	0.00%	0.00%

Table 4. Mesh accuracy tests.

For temperature (Figure 4a), the maximum normalized difference between numerical and experimental values is 12.3% in PT01, 4.6% in PT02 and 5.6% in PT03. Referring to the average experimental values, the relative gaps decrease to 6.3% (PT01), 1.7% (PT02) and 1.8% (PT03). Comparison of numerical temperature in PT01 with the experimental T_{mr} highlights a maximum normalized difference of 5.6% and a normalized deviation to the average value of 2.3%. Referring to RH (Figure 4b), a maximum absolute deviation of 6.3 (PT01), 4.8 (PT02) and 4.5 (PT03) percentage points, and an absolute deviation to the average value of 1.9, 2.9 and 3.4 percentage points, respectively can be found. Analysing the air velocity value, obtained under the plenum (Figure 4c), the detected range of variation is quite high with respect to the mean value (0.23 m/s), and the simulated velocity magnitude (0.27 m/s) highlights a consistent gap. However, it should be noticed that numerical values globally stand within the range of variation of the measurements, foregrounding a satisfactory agreement with the experimental data. A good agreement can be noted between microclimatic experimental with numerical results with relative differences lower than 10%. Comparison between microclimate experimental data with average parameter values, suggested by Italian and International standards, show that [47, 48, 49, 50,51, 32, 52] the average temperature values at probe locations are within the suggested limits. This is always confirmed for the "at rest" condition, but for the "operational" one, the acquired values exceed the recommended thresholds due to medical staff

presence and movements that produce local temperature and airflow modifications. The air velocity values globally fit the standard limits, suggested for unidirectional flow.

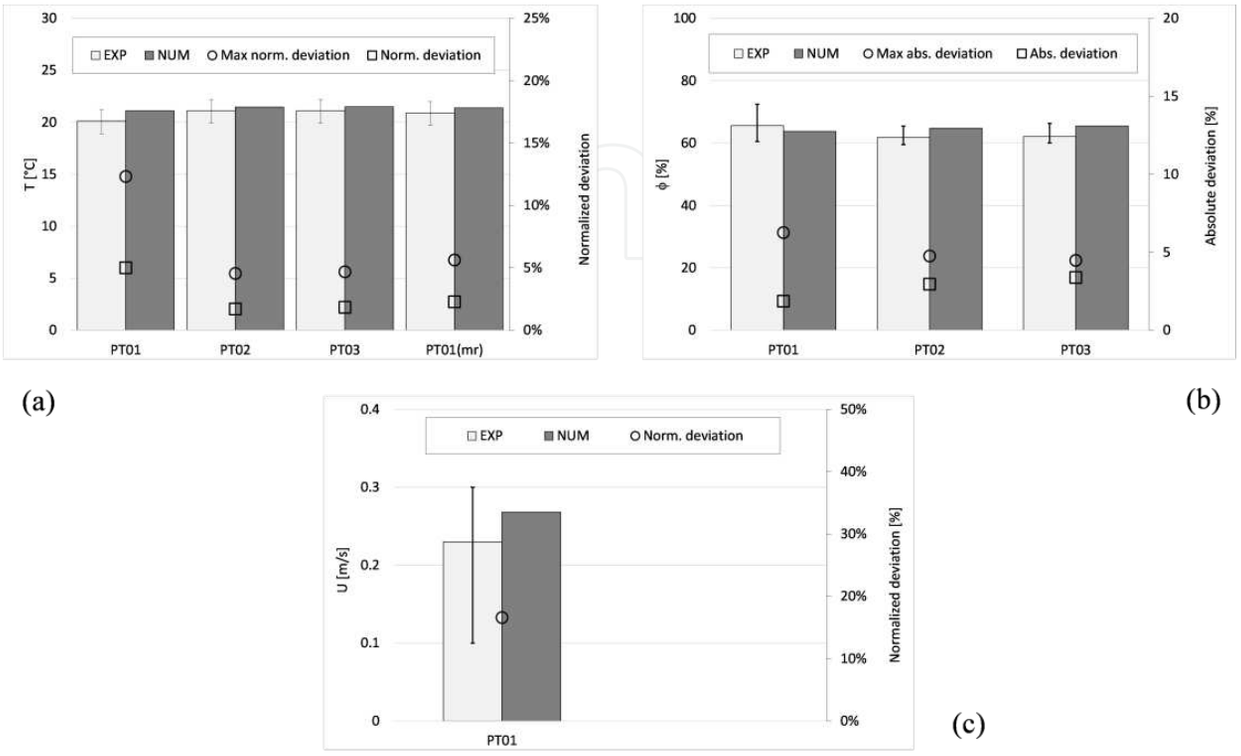

Figure 4. Comparison between numerical results (NUM, black grey) and mean-average experimental data (EXP, light grey). Error bars indicate the detected experimental deviation (minimum and maximum value). Circled and squared symbols (referring to the second y-axis) indicate the maximum deviation of numerical values from experimental data, and deviation of numerical results from experimental time averaged data, respectively. Temperature (a), RH (b) and velocity (c) values are reported at locations PT01, PT02 and PT03 (as shown in Figure 1).

4. Use of microbiological measurements for numerical model implementation and validation

Microbiological measurements of particle concentration were used to assess particle emission rates imposed as boundary conditions in the numerical models. Particle emission rate per person, distinguished for dimension, was not known a priori during our research. Zhao et al. [29] considered a constant generation rate of 0.0916 μg/s per person for each particle size group. For each particle dimension, referring to an assumed particle density of 1.05E-6 μg/μm^3, scaling the emission rate by the particle volume, it is possible to obtain the related number of particles emitted by a person in the time unit. Quian et al. [30] used a different method to assess particle emission rate, divided for different diameters, caused by the occupants in a classroom. They experimentally measured the particulate concentration at specific locations in the classroom for similar environmental conditions, but with and without people presence. They argued that

http://dx.doi.org/10.5772/59671

difference in acquisitions could be attributed to emissions due to occupant contribution, and then proposed a particulate emission distribution as a function of particle diameter. The emission rate refers to how many particles of a specific dimension are supplied by one person in the time unit to the surrounding environment. The two above mentioned approaches provide different results. In our investigation, we evaluated particle emission due to each occupant, differentiated for diameter dimension, using the experimental acquisitions of particle concentration in the real OT with and without patient and medical staff presence. In particular, we applied a similar method used in [30] to assess the particle emission rate by occupants to be used in the numerical models. Otherwise, in our case we combined the available experimental data with results coming out from numerical simulations to assess the emission rate of particles per person depending on particle dimension. The procedure used is given in the flow-chart diagram of Figure 5: the caption "sampling points" refers to points PT01, PT02, PT04 and PT05, "particle diameter range" means (0.3-0.5 μm); (0.5-1 μm); (1-5 μm), and "average particle diameter" refers to the average values of the particle diameter (0.4; 0.75; 3 μm) computed for each of the previous ranges.

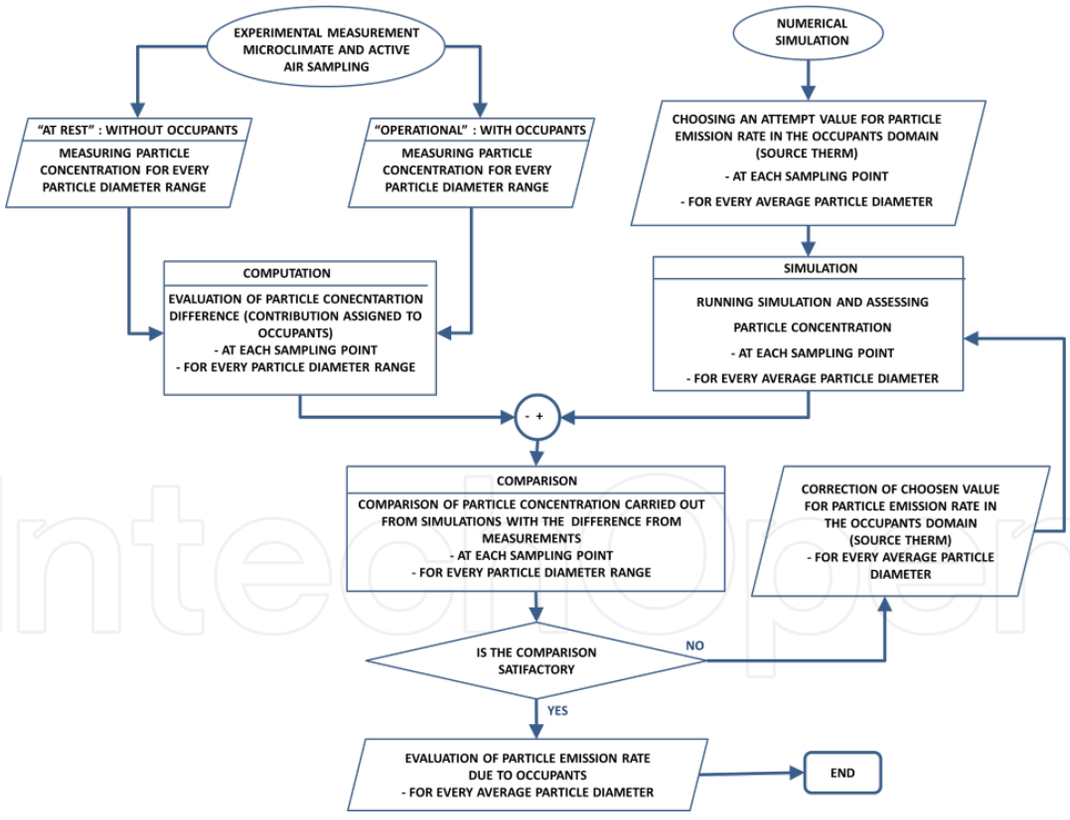

Figure 5. Flowchart of method used for estimating the occupant particle emission rate per diameter by an iterative cross-comparison between numerical and experimental data.

Comparison between experimental and numerical (NUM) particle concentration due to occupants in the OT is shown in Figure 6. In this figure, experimental value (EXP) for each

diameter (d_i) represents the difference between average data (Av) acquired for the at rest (rest) and operational (oper) conditions, computed as follows:

$$EXP_{d_i} = Av\left\{EXP_{d_i}\right\}_{oper} - Av\left\{EXP_{d_i}\right\}_{rest} \tag{3}$$

while the error bars are plotted by assuming the following:

$$Err_{d_i}^{+} = \max\left\{EXP_{d_i}\right\}_{oper} - \min\left\{EXP_{d_i}\right\}_{rest} \tag{4}$$

$$Err_{d_i}^{-} = \min\left\{EXP_{d_i}\right\}_{oper} - \max\left\{EXP_{d_i}\right\}_{rest} \tag{5}$$

Numerical values plotted, refer to the "final" particle emission rate per average diameter applied to the exposed person surfaces carried out from application of the computing procedure shown in Figure 5. Values of emission rate for diameter range are provided in Table 5, where values suggested in the previous literature are also reported.

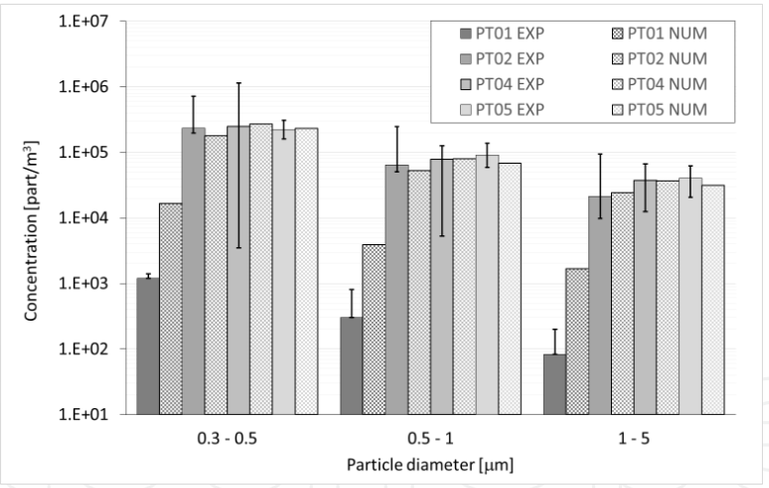

Figure 6. Particles concentration per diameter in different locations: comparison between experimental and numerical values.

Despite an iterative application of our proposed "guess and check" procedure, experimental/numerical difference in particle concentration at point PT01 remained quite high: the numerical model overestimates particle contents in the air at this location. Otherwise, a good agreement can be pointed out from comparison of particle concentration at the other different locations. Obtained results of particle emission rate per diameter and per person (Table 5), provide lower values with respect to those proposed by Quian et al. However, this is an expected result,

http://dx.doi.org/10.5772/59671

		Particle diameter [μm]							
		0.4	0.5	0.75	1	2	2.5	3	5
Present study	[part/s]	1.01E+05		2.96E+04				1.36E+04	
Zhao					1.67E+05		1.07E+04		1.33E+03
Quian		3.95E+06			7.58E+05		3.16E+05		2.43E+05

Table 5. Particle emission rate (particles/s) from persons differentiated by diameter.

because measurements by Quian [30] refer to a different indoor environment (university classroom) with different use conditions, occupied by students.

5. Numerical results

5.1. Microclimate and ventilation assessment

This chapter section is devoted to numerical results analysis and discussion. Figure 7-a-c provides the air velocity fields in a horizontal section (z=1.5) for the different room conditions studied. Transient simulation results (for the "incorrect use conditions", Figure 7c) refer to step 3, when the door is completely closed and the medical assistant walks through the room, until he reaches the top of the operating table. In particular, Figure 7c refers to the first 13 seconds, when the moving person has reached the table midpoint. Distribution of velocity magnitude in the operational zone is significantly modified from the "at rest" towards both the "operational conditions". In Figure 8a-c velocity profiles along x (y=8; z=1.5), y (x=3; z=1.5) and z (x=3; y=8) direction are given for the different room conditions. The "incorrect use conditions" still refer to the time instant t=13 s.

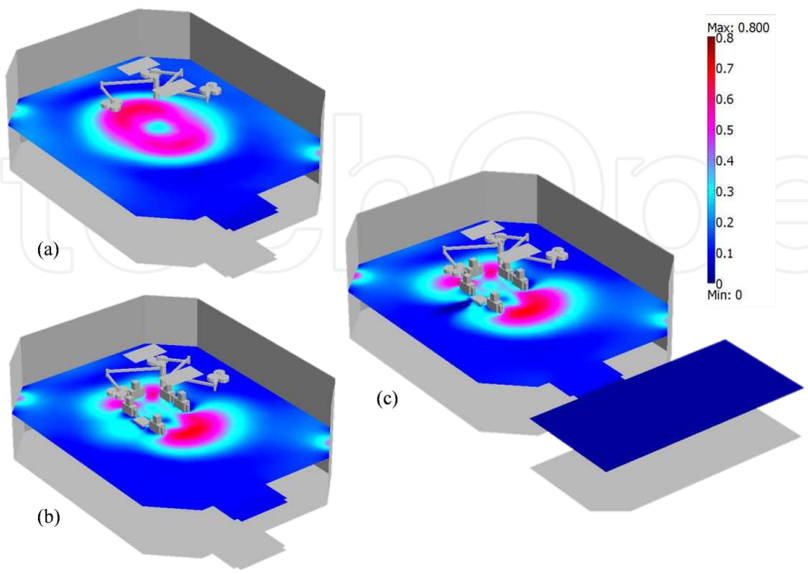

Figure 7. Air velocity field [m/s] in a horizontal plane (z=1.5) for "at rest" (a), "correct operational use" (b) and "incorrect operational use" (c).

In these diagrams zero values represent the "imprint" of a fixed object/person or moving person standing in that location for the considered instant. Velocity profiles underline the modifications of the air flow patterns due to the operational conditions. In particular, air flow in the surgical zone is strongly modified by medical staff presence: important differences, produced by this effect, are shown with the gap between dashed lines and continuous/dashed-dotted lines in Figs. 8a-8c.

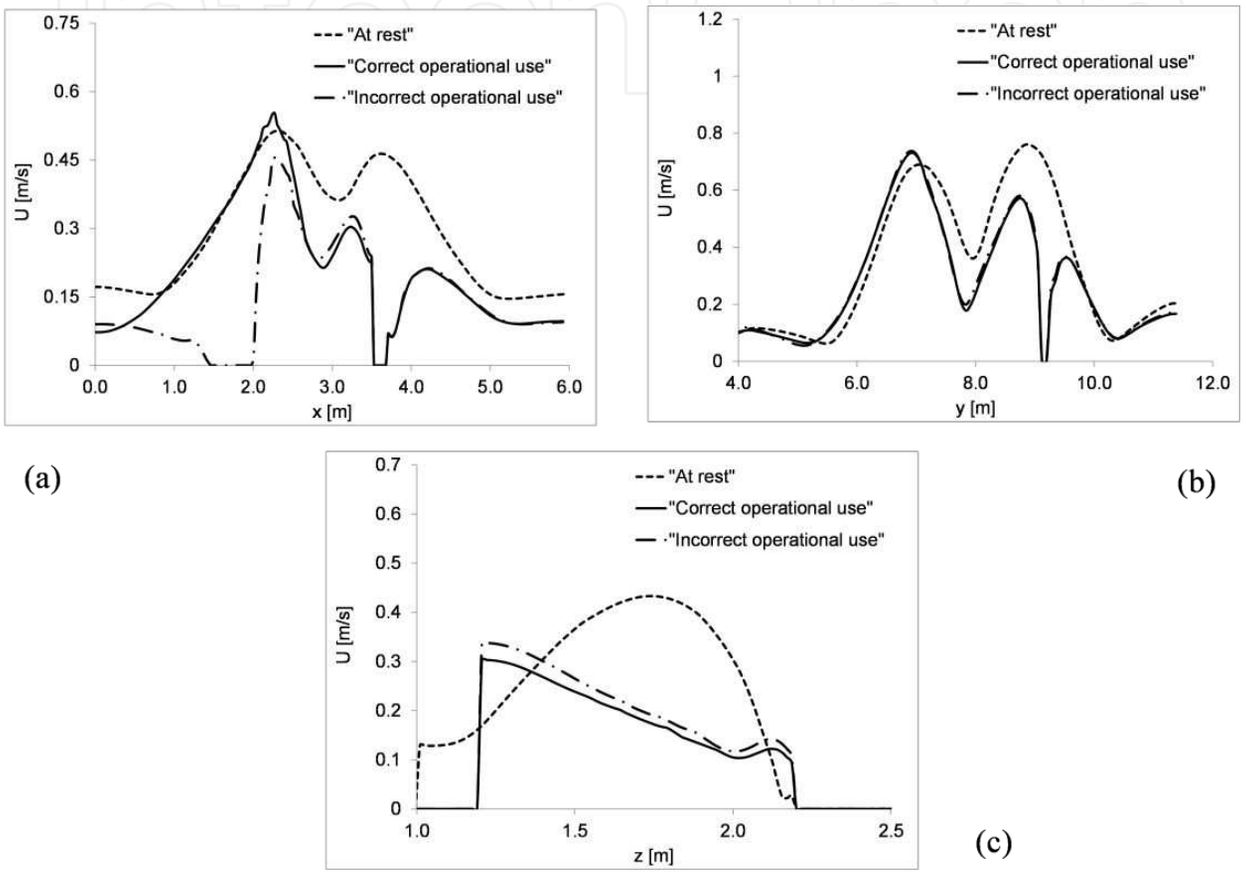

Figure 8. Velocity profiles for "at rest" (dashed line), "operational correct use (continuous line) and "operational incorrect use" (dotted-dashed line) along x (a) (y=8; z=1.5), y (b) (x=3; z=1.5) and z (c) (x=3; y=8).

The effect due to the person movements on the airflow patterns in the surgical zone, appears to be less important. In Figs.8b,8c continuous and dashed-dotted lines are almost overlapped, while in Figure 8a they are remarkably distant only for x<2.5. Velocity profiles show variable trends and high curve slopes in each case: this is really very important when the efficacy of "unidirectional" or "laminar" airflow is discussed for similar applications. Now the influence of OT use conditions on indoor thermal field variations, is discussed. Figure 9 shows the air temperature distribution by means of contour plots and horizontal slice (z=1.5), obtained for "incorrect use conditions", step 3, time 13 s. Thermal "imprint" of a walking person is clear. On the left side of Figure 9, thermal profiles obtained along the x axis (y=8; z=1.5, see the line sketch in the coloured map) for the different room conditions, is provided. Temperature variation is evident in the "correct operational use" compared with the empty room charac-

http://dx.doi.org/10.5772/59671

terized by a predominant isotherm profile. The additional thermal load, due to the walking person, produces a further local temperature increase. In the operating zone thermal levels remains very close to the design value despite the different use conditions. The mean air temperature value, computed all over the OT, is within the limits suggested by the Italian and International standards for the correct use conditions (23.5 °C) and slightly outside the limits for the incorrect use conditions (24.4 °C). Taking into account results obtained on the air RH, it can be detected that vapour production, due to persons presence, determines an air moisture content that is not well balanced by the incoming air at the considered hygrometric conditions. Figure10 shows (left side) RH distribution in a horizontal slice (z=1.5) for "correct operational conditions".

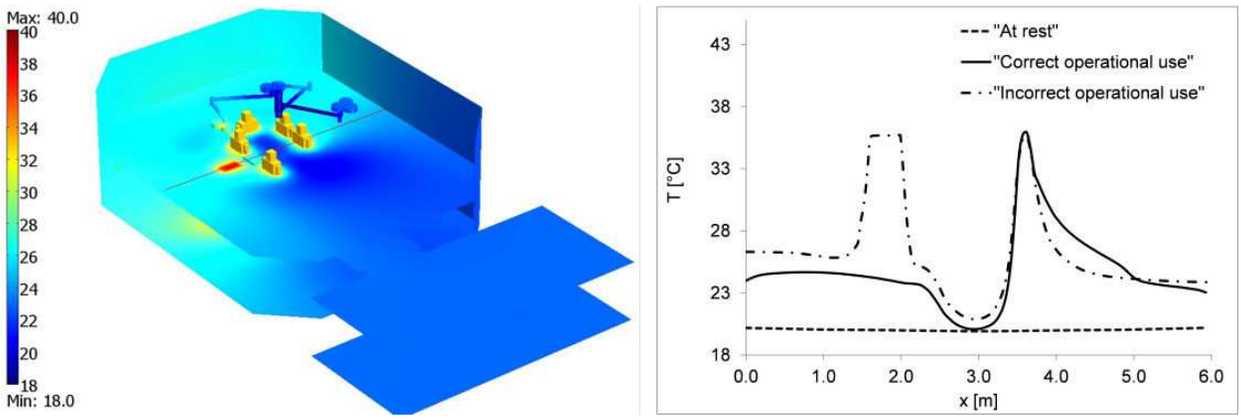

Figure 9. On the left side: temperature [°C] map plotted on contours and in a horizontal slice (z=1.5) for the "incorrect operational use" (step 3, time 13 s). On the right side: temperature profiles along the x-direction (y=8; z=1.5, see the line sketched on the slice) for "at rest" (dashed line), "operational correct use" (continuous line) and "operational incorrect use" (dotted-dashed line) conditions.

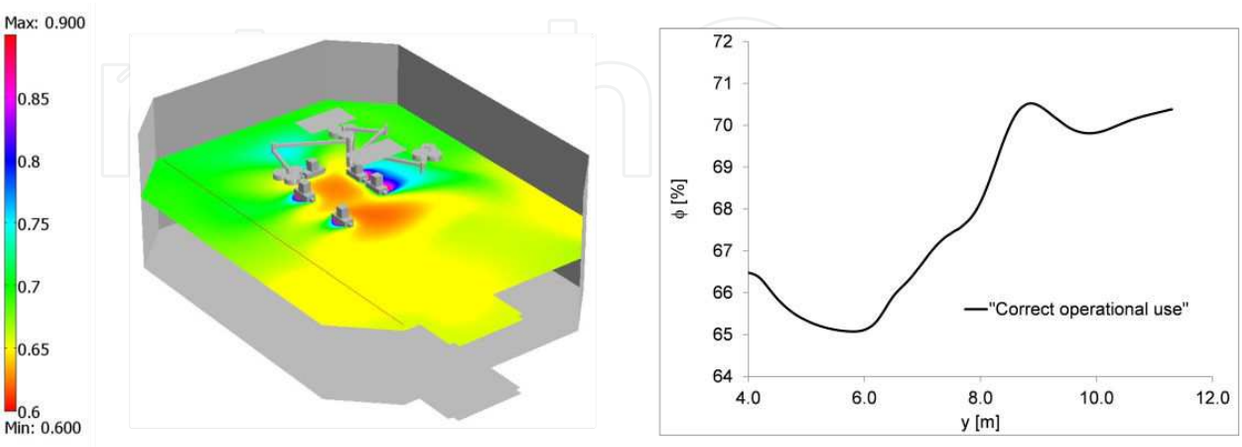

Figure 10. On the left side: RH (%) field in a horizontal plane (z=1.5) for the "correct operational use". On the right side: RH profile along the y-direction (x=1.1; z=1.5) for "operational correct use" (continuous line) conditions.

The mean value computed all over the room in this condition is 67.8%, which is exceeding any maximum threshold suggested by all the standards. The RH profile lying on a horizontal line along the y axis (x=1.1; z=1.5, sketched in the horizontal slice) is also reported in the right portion of Figure10. An increasing level of the moisture content along the y-direction can be noticed: RH at the back of the operating zone presents higher level. This could be due to the lack of ventilation all over the room that can determine stagnation zones. The mean age of air (τ) was also evaluated, using the steady airflow achieved for "at rest" and "correct operational conditions" as transport field for τ computations. The lower τ value corresponds to the higher air washing effect of the ventilation system for the considered zone. Results are plotted in Figure 11, where τ distribution is reported for both the analyzed conditions. In the same, the τ profiles along a horizontal line lying on the x direction (y=8; z=1.5, sketched on the horizontal slices) are provided. The τ values are not critical in both analyzed conditions. A much more uniform distribution is found for the empty room, and in this condition the medical staff act as a "constraint" for the local airflow, allowing a slightly lower air age value. It should be noticed that a lower air age does not directly mean better air quality. We were finally interested in assessing the effect of the sliding door opening/closing during the simulated "incorrect operational conditions". Figure12 provides the air velocity field on a horizontal plane (z=1.5) for step 2, at time 7 seconds: the medical assistant is walking in the room and the sliding door is shutting behind his back. In the same figure, as an enlargement, air velocity vector distribution is shown for the zone close to the sliding door. The important velocity field variation, in the zone of the sliding door, and also the one due to the medical assistant's movement through the room, is evident. As a consequence, an important rate of air outflows from the room. Then a total amount of 16.3 m^3 of air outflows toward the corridor during steps 5-6-7 (door opening/person crossing/door closing) was estimated.

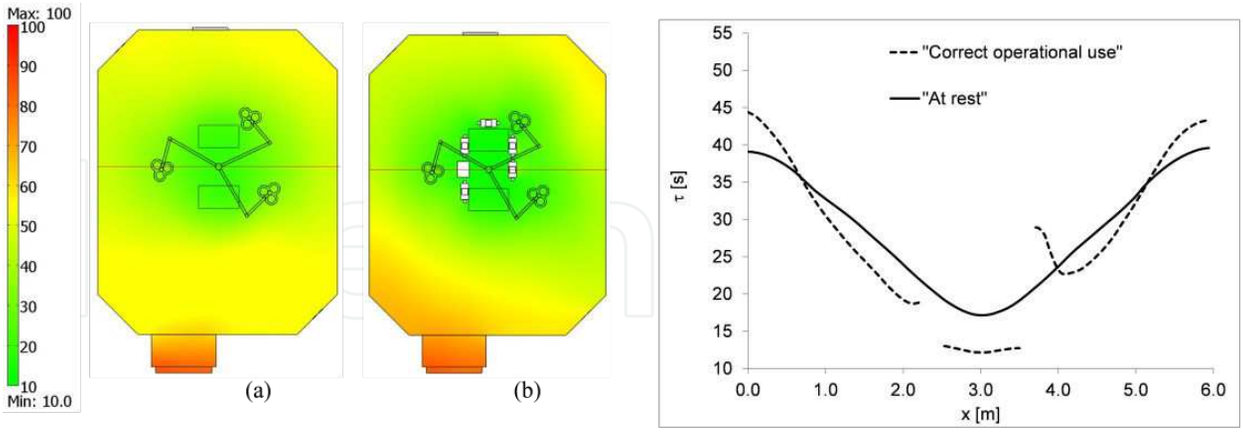

Figure 11. On the left side: mean age of air [s] in a horizontal slice (z=1.5) for the "at rest" (a) and "correct operational use" (b). On the right side: mean age of air profiles along the x-direction (y=8; z=1.5, see the line sketched on the slices) for "at rest" (continuous line) and "operational correct use" (dashed line) conditions.

Figure13 provides a representation of the airflow rate (continuous black line) and the total volume of air (grey-filled surface) outgoing the OT during the door opening. Indeed, the effect of the door opening on the average pressure level inside the OT was also investigated. Figure13

http://dx.doi.org/10.5772/59671

also shows the average pressure trend as a function of time during step 1 (door opening): a significant pressure decrease can be seen from the plotted data. Starting from its initial value, i.e. 32.6 Pa, the OT average overpressure with respect to the corridor level becomes very low, i.e. 1.2 Pa. The overpressure variation due to an "unforeseen event" occurring during an "incorrect use condition" of the OT, can determine a temporary non compliance of the pressure scheme with limits suggested by all the considered standards giving specific indications for it.

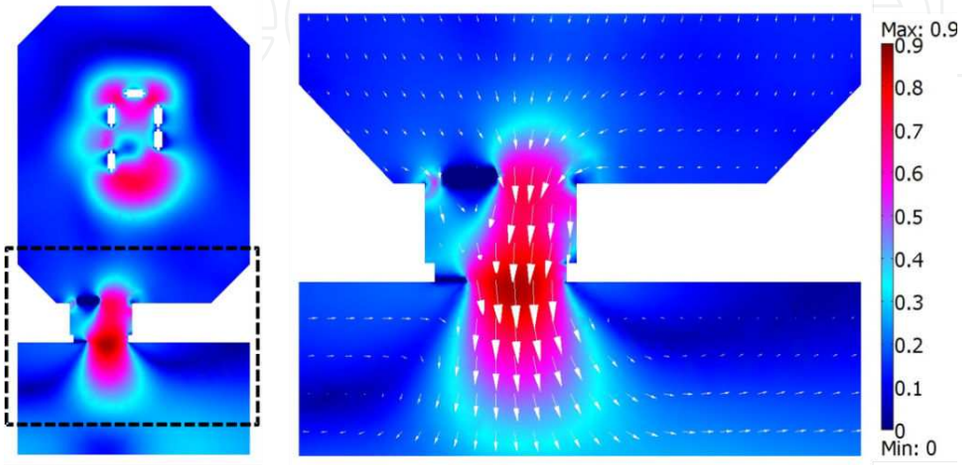

Figure 12. Air velocity field [m/s] in a horizontal slice (z=1.5) for step 2 and time 7 s (left side) and an enlargement with velocity vectors representation, in the proximity of crossing zone of the door towards the corridor (right side) during "incorrect operational use" conditions.

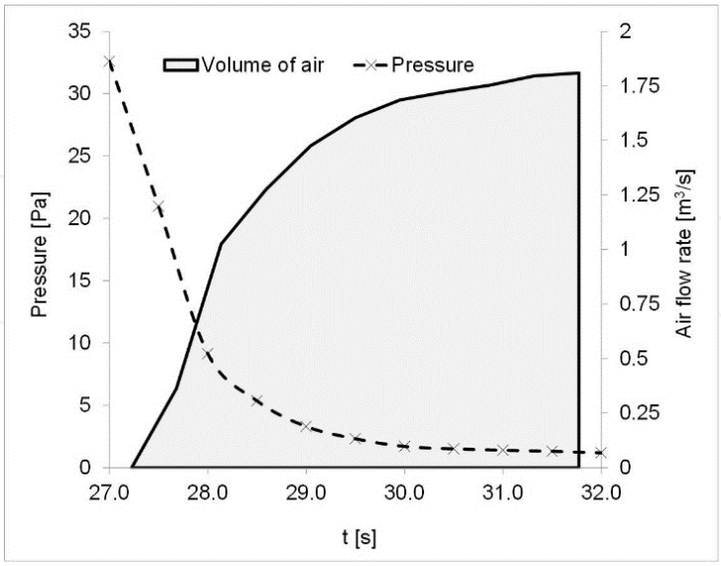

Figure 13. Time evolution of average OT pressure (dashed black line), airflow rate (continuous black line) and total volume of air out-coming the OT (grey-filled surface) during the sliding door opening (Step 5 of the "incorrect operational use" conditions).

5.2. IAQ indexes evaluation

Referring to the air freshness concept, the calculated CO_2 concentration, was found to be considerably below the critical limit of 3000 parts per million (ppm) in the global room volume and 1000 ppm in the operating table zone. CO_2 concentration is high only in the breathing zone where staff are exhaling. The driving effect due to the velocity field prevails over its spatial distribution. The simulation results obtained for CO_2 concentration and its distribution in the BZ and OZ, but also in the PZ and in the total volume of the OT, are in agreement with those provided by recent studies [15, 53]. Anyway, results showed that there is a significant increase in the CO_2 concentration from the fundamental zone BZ, to the OZ but progressively to the PZ and TV. Moreover, some IAQ indexes were computed using simulation results and discussed. The proposed indexes are usually applied for IAQ assessment and a quantitative evaluation of ventilation system performance with regard to contaminant removal and infection risk control [54, 55, 56]. Once the distribution of the dependent variables inside the OT, i.e. air velocity, CO_2 and particle concentration, were evaluated by simulations, IAQ indexes were calculated. Some of them were expressed in the form of a continuous distribution (local indexes), others were referred to the average values of dependent variables, in the BZ, OZ, PZ and TV. The first investigated IAQ parameter was the mean age of air (τ) [41, 42, 43]. The air age concept is generally defined as the average time for air to travel from a supply inlet area to any location in a forced ventilated room [57, 58, 59, 8]. The mean age of air was calculated as a dependent variable, as explained in the modeling section. It provides a measure of air freshness, so its lower values are more favourable. The τ parameter trend was controlled during a transient simulation of 1800 seconds, starting from an initial state corresponding to the steady state condition discussed in the above section. Figure 14 shows a spatial distribution of τ in a horizontal and in a vertical slice of the room, once the transient time to achieve the steady state was expired. Results show that lifetime of air located in the central portion of the OT is much lower than that concerning the peripheral portion of the room (Figure 14).

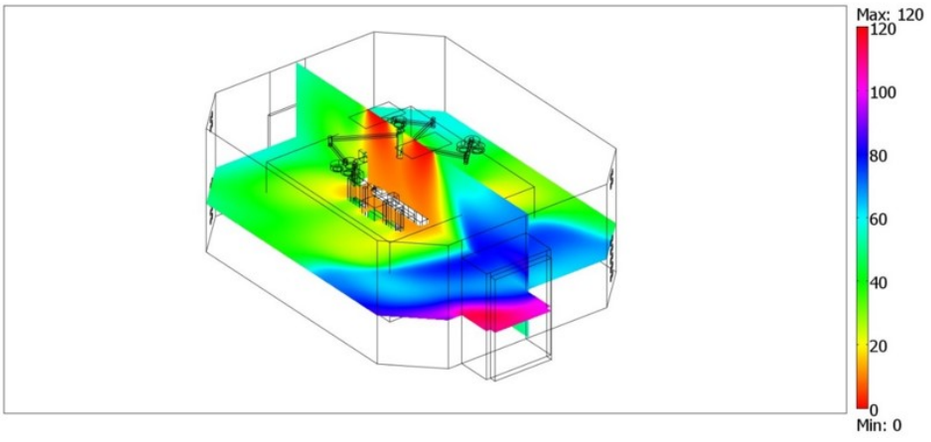

Figure 14. Mean age of air in horizontal (z=1) and vertical (x=3.0) slices.

To quantify this result, the average value of τ was computed in the OT different zones (i.e. BZ, OZ, PZ, TV), and called as τ_{Zj}, where Zj means the generic j-zone (Table 6). Generally, these

http://dx.doi.org/10.5772/59671

values are quite low. Comparison of these values with the theoretical residence time of air inside the OT (defined as the ratio between the total volume of the room (V_{TV}, m^3) and the mass flow rate of incoming ventilating air (V_{vent}, m^3/s)), shows that the ratio is always higher than 1.

	BZ	OZ	TV	PZ
τ_{ZJ} [s]	25.6	27.7	46.3	51.1
ACE [-]	210%	194%	116%	105%

Table 6. Values of mean age of air and Air Change Efficiency in the different zones.

Indeed, this comparison consists in computing the following Air Change Efficiency (ACE) index:

$$ACE = \frac{V_{TV} / \dot{V}_{vent}}{\tau_{Z_j}} \cdot 100 \tag{6}$$

whose values in the different zones are given in Table 6. The ACE index measures how effectively ventilation systems replace the air in a room with fresh air. In the BZ the average lifetime of air is more than 2 times lower than the theoretical residence time (about 53.7 seconds), that can be deduced analytically. The Local Air Change Efficiency (LACE) is expressed by the following expression:

$$LACE = \frac{V_{TV} / \dot{V}_{vent}}{\tau} \cdot 100 \tag{7}$$

The LACE index characterizes the conditions at a specific point (defined as the ratio between the minimum replacement time, as previously defined, and the local mean age of the air). It is possible to observe (Figure15) that the zone corresponding to the operating table is more favourable from this point of view, reaching LACE values of up to 500-600%.

Knowing the concentration field computed for CO_2 and particles, the Ventilation Effectiveness (VE) index was also assessed. The VE index measures how quickly a contaminant is removed from an air volume by quantifying the efficiency with which the internal pollutant is diluted or removed. It depends on the airflow patterns, and is expressed as follows:

$$VE = \frac{C_E - C_S}{C_{Z_j} - C_S} \tag{8}$$

where C_E is the mean value of contaminant concentration (i.e. CO_2 and particles) calculated at the air-recovery grilles (Exhaust), C_S is the contaminant concentration at the air inlet diffusers (Supply) and C_{Zj} is the mean value of the contaminant concentration in a specific OT zone (i.e. BZ, OZ, PZ, TV).

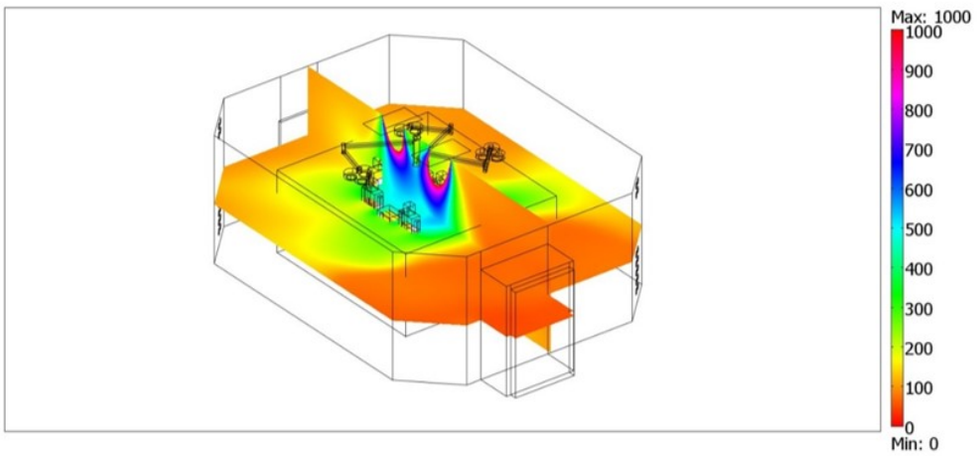

Figure 15. LACE index in horizontal (z=1.2) and vertical slices (x=3.0).

Similarly, the Contaminant Removal Effectiveness (CRE) index, expressed by the ratio between the concentration of contaminants at the exhaust point and the mean value of contaminant concentration within a specific zone was evaluated:

$$CRE = \frac{C_E}{C_{Z_j}} \tag{9}$$

Figure 16 shows the VE and CRE indexes, computed using CO_2 and particle concentrations. Because the particle concentration value was assumed to be zero at the inlet air diffusers (C_S=0), VE and CRE expressions correspond to each other. Due to the very low effect of the settling velocity on particle concentration distribution, a very low quantitative difference was found in computing the CRE (or VE) index as a function of the different particle diameter ranges studied. Therefore, we referred to a single CRE index representative for any particle diameter range studied. Values of the computed global indexes are shown in Figures 17 (CO_2) and 18 (particles). The CRE distribution at a specific point, that is known as Local Contaminant Removal Effectiveness (LCRE) was also calculated by:

$$LCRE = \frac{C_E}{C} \tag{10}$$

http://dx.doi.org/10.5772/59671

Local index distributions are shown in Figure 17 for CO_2 and in Figure 18 for the particles concentration. Comparison between the LCRE indexes, computed for CO_2 and particles, highlights the combined effect of the two sources (nose for CO_2 and body surface for particles) which provides very different trends. The mass transport effect is particularly evident in both cases.

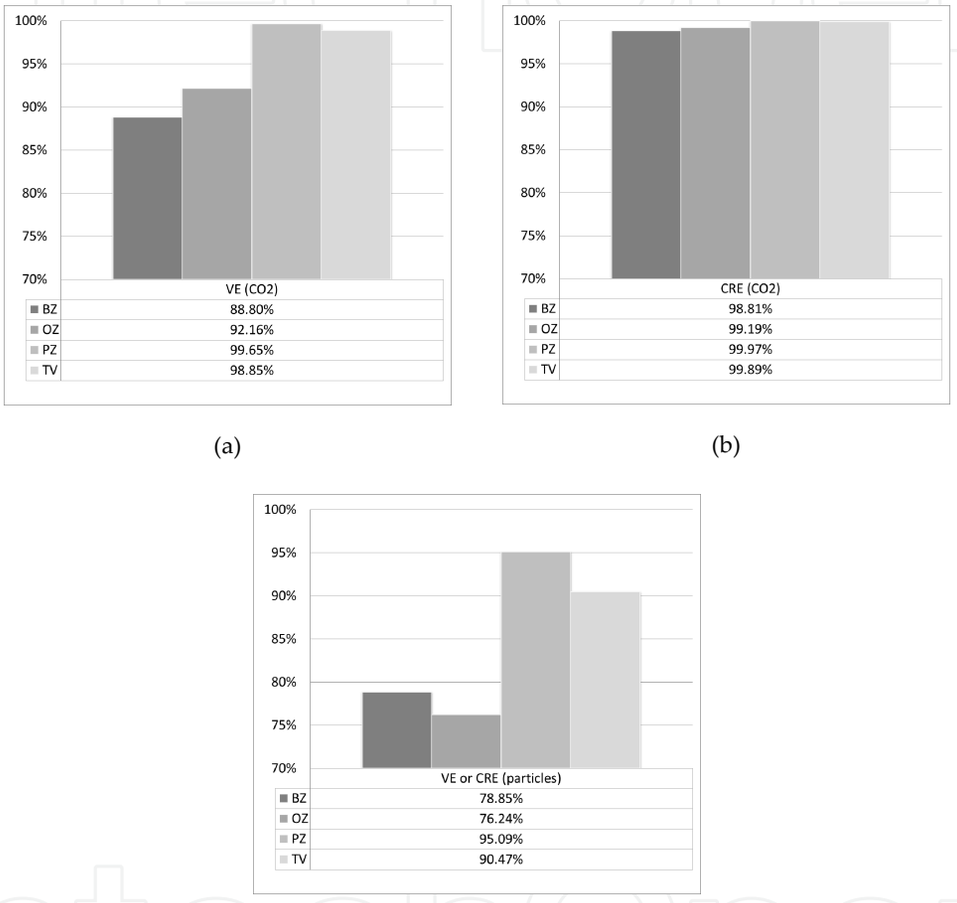

Figure 16. VE (a) and CRE (b) computed for CO_2 concentration in the different zones and VE (or CRE) computed for particles concentration in the different zones (c).

6. Conclusions

An experimental and numerical investigation on the airflow patterns and thermal field in a real OT is presented in this chapter. Different scenarios were considered, then measured and simulated, representative of "at rest" and "operational/effective use" conditions of the OT.

Numerical models were successfully validated against experimental data. In this chapter crucial results of our investigation, obtained through comparison and discussion of quantitative microclimatic parameters (air velocity, temperature, RH and pressure) the influence of unforeseen movements of medical staff, sensible and latent heat, but also CO_2 and particles, released by persons in the ambient and sliding door opening/closing on the OT climate and IAQ, are provided. It can be noticed that, variations in use (resulting in different internal sensible and latent heat loads, moving objects and room confinement) can play an important role in terms of microclimatic system performance against standard suggestions, even those lacking compliance with standard limits are found to be mainly local or temporary.

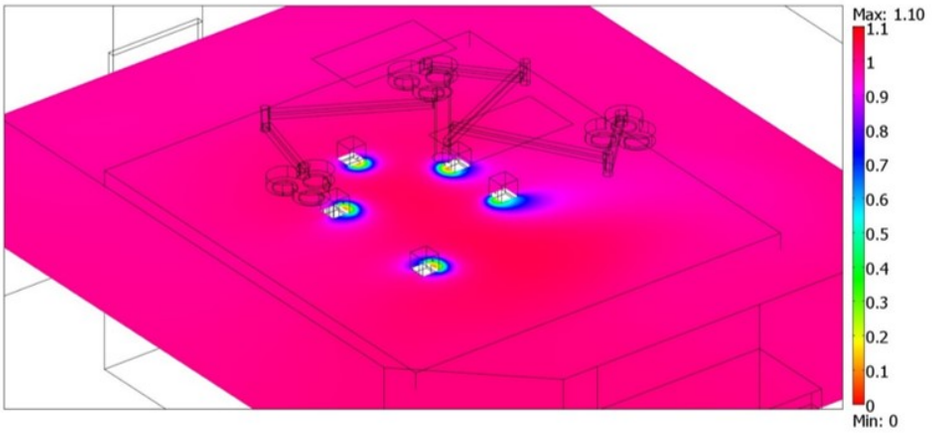

Figure 17. LCRE for CO_2 in a horizontal slice (z=1.6).

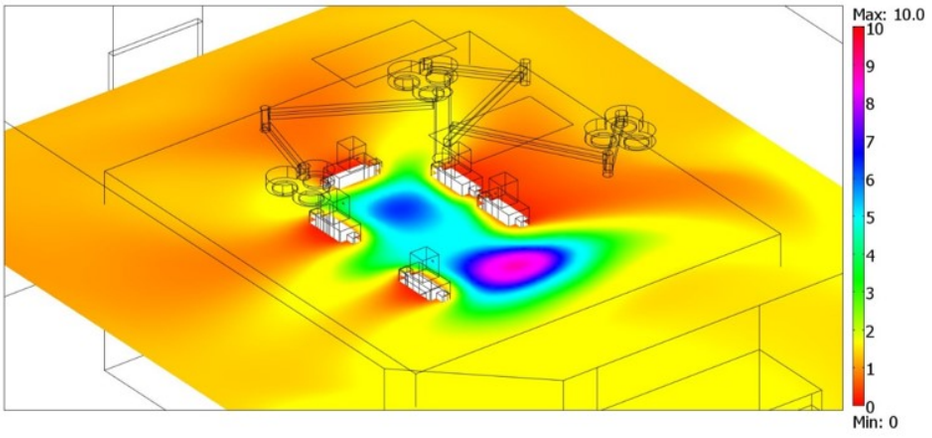

Figure 18. LCRE for particles concentration in a horizontal slice (z=1.4).

From the case study presented here, the efficiency of the AHU-HVAC system for providing the right indoor microclimatic conditions in compliance with standard thresholds is seen not only related to a good plant design, but also to medical staff and assistant behaviour and room use. Measurements of particle concentration, with and without persons, are used in combination with iteratively computed numerical results in order to assess particle emission rate by the

http://dx.doi.org/10.5772/59671

occupants for given particle dimensions. Particle concentration fields are also numerically solved for several particle diameters, by using an Euler approach based on the Cunningham formulation of settling velocity. Numerical results are successfully checked against the experimental evidence. CO_2 concentration levels numerically computed in the OT agree well with data reported in the literature for similar applications. Some consolidated indexes, adopted for monitoring the IAQ, are computed for gaseous contaminant (CO_2) and particle concentration, both in terms of spatial distribution and overall values referring to specific OT zones. Results obtained, by applying our proposed methodology for estimating the particle emission rate, highlight a good agreement with the small number of contributions in the literature concerning particle emission for different diameters. Our study contributes to better understanding the additional environmental "load" induced by the medical staff in an OT, based on an innovative strategy proposed and applied to quantify the particle emission rate released by occupants, for given ranges of particle diameters. Our integrated experimental and numerical approach, is in accordance with some recent surgical infection control guidelines, that highlight the importance of surgical staff behaviour control in order to decrease air contamination and wound colonisation. These recommendations include restricting the movements and the number of persons in the OT, but they are often general and based on expert advice. An integrated approach, such as that proposed here, based on CFD application and periodic experimental monitoring campaigns of OT, can contribute to providing valuable suggestions for medical staff information and education concerning the analysed topics, and in general can hopefully stimulate careful considerations on specific procedures for OT design and use.

Nomencalture

Symbol		S.I. Unit
C_p	Specific heat at constant pressure	[J/(kg K)]
D_w	Vapour diffusivity	[m^2/s]
F	Magnitude of buoyancy force	[N/m^3]
h	Coefficient of heat transfer	[W/(m^2 K)]
$\mathbf{I}$	Identity tensor	
k	Turbulent kinetic energy	
p	Pressure	[Pa]
$\mathbf{n}$	Normal unit vector	
M	Vapour production	[kg/(s m^3)]
Q	Sensible heat source	[W/m^3]
$\mathbf{U} \equiv (u, v, w)$	Velocity vector	[m/s]
U	Magnitude of velocity vector	[m/s]
t	Time	[s]
T	Temperature	[K]

Greek symbols

δ_p	Vapour permeability in the air	[kg/(m s Pa)]
δ_w	Wall offset	[m]
ε	Dissipation rate of turbulent kinetic energy	[-]
ϕ	Relative humidity	[%]
ι	Percentage error	[-]
κ	Karman's constant	[-]
ξ	Moisture capacity	[kg/m^3]
λ	Thermal conductivity	[W/(m K)]
μ	Dynamic viscosity	[Pa s]
ρ	Density	[kg/m^3]
σ	Standard deviation	
τ	Mean age of air	[s]

Subscript

AV	Average
in	Incoming
MAX	Maximum
MIN	Minimum
neigh	Neighbouring
mr	Mean radiant
out	Outgoing
sat	Saturation
T	Turbulent

Acknowledgements

The Authors thank Prof. Pietro Vitali (Hospital Hygiene Unit, University Hospital of Parma), Prof. Cesira Pasquarella (Department of Biomedical, Biotechnological and Translational Sciences, University of Parma), Prof. Roberto Albertini (Department of Clinical and Experimental Medicine, Unit of Medical Immunology, University Hospital of Parma), Prof. Giuliano Cammarata (Department of Industrial Engineering, University of Catania) for their crucial cooperation and research support. The authors want also to thank the PhD students engaged for the hip surgery simulation and indoor microclimatic measurements, active and passive air samplings.

http://dx.doi.org/10.5772/59671

Author details

Carla Balocco[1] and Giuseppe Petrone[2]

1 Department of Industrial Engineering, University of Firenze, Firenze, Italy

2 Department of Industrial Engineering, University of Catania, Catania, Italy

References

[1] Chow TT, Yang XY. Performance of ventilation system in a non-standard operating room. Building and Environment 2003; 38(12) 1401-1411.

[2] Chow, T.T., Fog, K.F., Tsang, C.F., Qiuwang, W. Comparison of performances of displacement and mixing ventilations. Part II: indoor air quality. Int.J. of Refrigeration 2005; 28 288-305.

[3] Karthikeyan CP, Samuel Anand A. CO_2 dispersion studies in an operation theatre under transient conditions. Energy and Buildings 2008; 40 231-239.

[4] Pfost JF. A re-evaluation of laminar air flow in hospital operating rooms. ASHRAE Transactions 1981; 87(2) 729-739.

[5] Ho SH, Rosario L, Rahman MR. Three-dimensional analysis for hospital operating room thermal comfort and contaminant removal. Applied Thermal Engineering 2009; 29 2080-2092.

[6] Memarzadeh F, Manning A. Comparison of operation room ventilation systems in the protection of surgical site. ASHRAE Transactions 2002; 108(22) 3-15.

[7] Memarzadeh F, Manning A. Reducing risks of surgery. ASHRAE Journal 2003 ; 45(2) 28-33.

[8] Mendez C, San Jose´ JF, Villafruela JM, Castro F. Optimization of a hospital room by means of CFD for more efficient ventilation. Energy and Buildings, 2008; 40 849–854.

[9] Chow TT, Zhang L, Wei B. The integrated effect of medical lamp position and diffuser discharge velocity on ultraclean ventilation performance in an operating theatre. Indoor Built Environment 2006; 15(4) 315-331.

[10] Zoon WAC, Van der Heijden HGM, Loomans MGLC, Hensen JLM. On the applicability of the laminar flow index when selecting surgical lighting. Building and Environment 2010; 45(9) 1976-1983.

[11] Zoon WAC, Loomans MGLC, Hensen JLM. Testing the effectiveness of operating room ventilation with regard to removal of airborne bacteria. Building and Environment 2011; 46 2570-2577.

[12] Kameel R, Khalil EE. Experimental and numerical investigations of airflow regimes in air-conditioned operation theatres. Proc. 14th Usnctam, Symposium On Recent Advances In Three Dimensional Flow Modeling 2003; Paper 52.

[13] Dong S, TU G, CAO R, YU Z. Numerical study on effects of door-opening on airflow patterns and dynamic cross-contamination in an ISO class 5 operating room. Trans. Tianjin Univ. 2009; 15 210-215.

[14] Shih YC, Chiu CC, Wang O. Dynamic airflow simulation within an isolation room. Building and Environment 2007; 42 3194-3209.

[15] Santa Cruz A, Guillou S, Makhloufi R. Effect of moving person on airflow patterns in a ventilated enclosure (operating theatre applications). ITBM RBM 2007; 28 49-55. (In French).

[16] Yang SJ, Fu WS. A numerical investigation of effects of a moving operator on airflow patterns in a cleanroom. Building and Environment 2002; 37 705-712.

[17] Brohus H, Balling KD, Jeppesen D. Influence of movements on contaminant transport in an operating room. Indoor Air 2006; 16 356–372.

[18] Balocco C, Petrone G, Cammarata G. Assessing the effects of sliding doors on an operating theatre climate. Building Simulation: An International Journal 2012; 5(1) 73-83.

[19] Balocco C, Petrone G, Cammarata G. Numerical multi-physical approach for the assessment of coupled heat and moisture transfer combined with people movements in historical buildings. Building Simulation: An International Journal 2013; 5(1) 73-83

[20] Chow, TT, Wang, J. Dynamic simulation on impact of surgeon bending movement on bacteria-carrying particles distribution in operating theatre. Building and Environment 2012; 57 68-80

[21] Franke, JE, Wadden RA. Indoor Contaminant Emission Rates Characterized by Source Activity Factors, Environmental Science and Technology 1987; 21 45-51

[22] Friberg B, Friberg S, Östensson R, Burman LG. Surgical area contamination-comparable bacterial counts using disposable head and mask and helmet aspirator system, but dramatic increase upon omission of head-gear: an experimental study in horizontal laminar air-flow, Journal of Hospital Infection 2001; 47 110-115.

[23] Hospodsky D, Qian J, Nazaroff WW, Yamamoto N, Bibby K, Yazdi HR, Peccia J. Human Occupancy as a Source of Indoor Airborne Bacteria, Plos One Sources of Indoor Airborne Bacteria 2012; 7(4) 1-10.

[24] Nazaroff, WW. Indoor particle dynamics. Indoor Air 2004; 7 175-183.

[25] Li Chih-Shan, Hou Po-An. Bioaerosol characteristics in hospital clean rooms. The Science of the Total Environment 2003; 305 169–76.

[26] Yu BF, Hu ZB, Liu M, Yang HL, Kong QX, Liu YH. Review of research on air-conditioning systems and indoor air quality control for human health, International Journal of Refrigeration 2009; 32 3-20.

[27] Chen FZ, Yu Simon CM, Lai Alvin CK. Modeling particle distribution and deposition in indoor environments with a new drift-flux model. Atmospheric Environment 2006; 40 357-367.

[28] Gao NP, Niu JL. Modeling particle dispersion and deposition in indoor environments, Atmospheric Environment 2007; 41 3862-3876.

[29] Zhao B, Zhang Y, Lia X, Yang X, Huang D. Comparison of indoor aerosol particle concentration and deposition in different ventilated rooms by numerical method, Building and Environment 2004; 39 1-8.

[30] Qian J, Hospodsky D, Yamamoto N, Nazaroff WW, Peccia J. Size-resolved emission rates of airborne bacteria and fungi in an occupied classroom, Indoor Air 2012; 22 339–351.

[31] ANSI/ASHRAE Standard 62.1-2007, Ventilation for Acceptable Indoor Air Quality

[32] HTM 03-01-2007. Heating and ventilation systems Health Technical Memorandum 03-01: Specialised ventilation for healthcare premises Part A: Design and validation. Edinburgh, UK: TSO.

[33] UNI EN ISO 14644-3-2006. Cleanrooms and associated controlled environments - Part 3: Test Methods.

[34] UNI EN ISO 14644-1-1999. Cleanrooms and associated controlled environments - Part1: Classification of air cleanliness (ISO 14644-1:1999)

[35] UNI 11425-2011. Surgery operating theatre, ventilation and air-conditioning system for contamination control (VCCC) - Design, construction, commissioning, qualification, management and maintenance. (In Italian).

[36] ANSI/ASHRAE Standard 62.1-2004 Ventilation for Acceptable Indoor Air Quality

[37] ANSI/ASHRAE Standard 55-2005 Thermal Environmental Conditions for Human Occupancy.

[38] Comsol. Introduction to COMSOL Multiphysics. 2012; v. 4.3. http://www.comsol.com/.

[39] Ignat L, Pelletier D, Ilinca F. A universal formulation of two-equation models for adaptive computation of turbulent flows. Computer Methods in Applied Mechanics and Engineering 2000; 189 1119–1139.

[40] Launder BE, Spalding DB. The Numerical Computation of Turbulent Flows. Computer Methods in Applied Mechanics and Engineering 1974; 3 269-289.

[41] Abanto J, Rarrero D, Reggio M, Ozell B. Air flow modelling in a computer room. Building and Environment 2004; 391393-1402.

[42] Zhang L, Chow TT, Fog KF, Tsang CF, Qiuwang W. Comparison of performances of displacement and mixing ventilations. Part II: indoor air quality. International Journal of Refrigeration 2005; 28 288-305.

[43] Petrone G, Cammarata L, Cammarata G. A multi-physical simulation on the IAQ in a movie theatre equipped by different ventilating systems. Building Simulation: An International Journal 2011; 4 21-31.

[44] Hinze JO. Turbulence. 2nd ed. New York: McGraw Hill; 1975.

[45] Deuflhard P. A modified Newton method for the solution of ill-conditioned systems of nonlinear equations with application to multiple shooting. Numerical Mathematics 1974; 22 289-315.

[46] Hindmarsh H, Brown AC, Grant PN, Lee KE, Serban SL, Shumaker R, Woodward DE, Woodward CS. SUNDIALS: Suite of Nonlinear and Differential/Algebraic Equation Solvers. ACM Trans. Math. Software 2005; 31 363-396.

[47] ONORM H 6020-2007. Ventilation and air conditioning plants for locations for medical use - Design, construction, operation, maintenance, technical and hygienic inspections.

[48] VDI 2167-2004. Part 1. Building services in hospitals – Heating, ventilation and air-conditioning

[49] DPR 14-01-1997. Approvazione dell'atto di indirizzo e coordinamento alle regioni e alle province autonome di Trento e di Bolzano, in materia di requisiti strutturali, tecnologici ed organizzativi minimi per l'esercizio delle attività sanitaria da parte delle strutture pubbliche e private. In: G.U.R.I. 20/02/1997 n.42. (In Italian).

[50] ISPESL-2009. Dipartimento Igiene del Lavoro, Linee guida per la definizione degli standard di sicurezza e di igiene ambientale dei reparti operatori. http://www.ispesl.it/. (In Italian).

[51] NBHF-2004. Building guidelines for a surgical department.

[52] ANSI/ASHRAE 170-2008. Ventilation of Health Care Facilities.

[53] Al-Waked R. Effect of ventilation strategies on infection control inside operating theatres. Engineering Application of Computational Fluid Mechanics 2010; 4(1) 1-16.

[54] Villafruela JM, Castro F, San José JF, Saint-Martin J. Comparison of air change efficiency, contaminant removal effectiveness and infection risk as IAQ indices in isolation rooms. Energy and Buildings 2013; 57 210-219.

[55] Kwon KS, Lee IB, Han HT, Shin CY, Hwang HS, Hong SW, Bitog J P, Seo IH, Han CP. Analysing ventilation efficiency in a test chamber using age-of-air concept and CFD technology. Biosystems Engineering 2011; 110 421-433.

[56] Meiss A, Feijo-Mu˜noz J, Garcia-Fuentes MA. Age-of-the-air in rooms according to the environmental condition of temperature: A case study. Energy and Buildings 2013; 67 88-96.

[57] Sandberg M, Sjöberg M. The use of moments for assessing air quality in ventilated rooms. Building and Environment 1983; 18(4)181–197.

[58] Federspiel CC. Air-change effectiveness: theory and calculation methods. Indoor Air 1999; 9 47–56.

[59] Xianting Li, Dongning Li, Xudong Yang, Jianrong Yang. Total air age: an extension of the air age concept. Building and Environment 2003; 38 1263 – 1269.

IntechOpen